JOURNAL OF GEOPHYSICAL RESEARCH, VOL. 90, NO. C1, PAGES 1005–1018, JANUARY 20, 1985

A Comparison of in Situ and Airborne Radar Observations of Ocean Wave Directionality

FREDERICK C. JACKSON AND W. TRAVIS WALTON[1]

NASA Goddard Space Flight Center, Greenbelt, Maryland

CHICH Y. PENG

Science Systems and Applications, Inc., Seabrook, Maryland

The directional spectrum of a fully arisen ~3 m sea as measured by an experimental airborne radar, the NASA K_u-band radar ocean wave spectrometer (ROWS), is compared to reference pitch-roll buoy data and to the classical SWOP (stereo wave observation project) spectrum for fully developed conditions. The ROWS spectrum, inferred indirectly from backscattered power measurements at 5-km altitude, is shown to be in excellent agreement with the buoy spectrum. Specifically, excellent agreement is found between the two nondirectional height spectra, and mean wave directions and directional spreads as functions of frequency. This agreement is found despite certain discrepancies between the radar and buoy angular harmonics which are believed to be due to buoy instrumental effects. A comparison of the ROWS and SWOP spectra shows the two spectra to be very similar, in detailed shape as well as in terms of the gross spreading characteristics. Both spectra are seen to exhibit bimodal structures which accord with the Phillips' resonance mechanism. This observation is thus seen to support Phillips' contention that the SWOP modes were indeed resonance modes, not statistical artifacts.

INTRODUCTION

Progress in understanding the physics of wind-generated ocean waves, and in our ability to model and forecast them has long been hampered by a lack of adequate observations. This is especially true regarding directional wave observations. For example, the directional spreading characteristics of growing waves even under ideal fetch-limited conditions are basically unknown, the few extant observations being in complete disagreement with each other [*Kuik and Holthuijsen*, 1982] The response of a wave field to a rapidly varying wind field is basically an open question, and one that is difficult to resolve without directional observations [*Hasselmann*, 1984]. Current theory, which would ascribe to conservative, nonlinear wave-wave interactions a strong directional coupling between components, is unsupported, if not contradicted, by observation [*Holthuijsen*, 1983]. While the need for directional wave data is clear, both from scientific and applications viewpoints, present technology is hard-pressed to provide the necessary data [*Dean*, 1982]. The difficulties in developing practical, deep-water in situ directional wave sensors are well known, as are the practical limitations to conventional remote sensing techniques such as stereo photography [*Coté et al.*, 1960; *Holthuijsen*, 1983], and this situation is not likely to change in the foreseeable future.

There has been some recognition in recent years of the potential of airborne and satellite microwave radars for large-area coverage, high resolution directional wave spectrum measurements [*Dean*, 1982]. Yet, presently, no truly remote microwave sensing technique has gained general acceptance in the oceanographic or ocean engineering communities. The problems inherent to spaceborne synthetic aperture imaging radar (SAR), often merely in imaging a wave field, are well known [cf. *Alpers et al.*, 1981]. Neither real aperture side-looking airborne radar (SLAR) nor SAR imaging radar techniques have yet received a credible comparison with in-situ instrumentation. Most all comparisons made to date have been simply in terms of measured dominant wavelengths and directions, rather than in terms of the actual directional spectra. Exceptions to this rule include papers by *Pawka et al.* [1980] and *McLeish and Ross* [1983], in which comparisons were made in terms of normalized directional distributions.

(The term "truly remote" ought perhaps to be defined. By this we mean any remote measurement that requires a scattering model to infer surface properties. Only such indirect measurements are feasible from satellites. The NASA surface contour radar [*Walsh et al.*, 1982], since it measures the surface elevation topography directly by ranging, is not, according to this definition, a "truly" remote sensor).

The two major sources of difficulty (apart from the technological) with the imaging radar approach to ocean waves measurement are (1) the Doppler phase histroy distortion caused by the motion of the surface (most severe for spaceborne SAR's), and (2) the complex and basically unpredictable nature of the relationship between the surface reflectivity field and the wave height which exists in the large-angle Bragg scatter regime in which most imaging radars are operated. *Jackson* [1981] showed how both of these problems that have so much preoccupied the radio oceanographic community may be circumvented. First, the wave motion problem in the spaceborne SAR technique is obviated in a real aperture system that obtains wave directionality by azimuth-scanning the antenna beam (this approach has the limitation of requiring fairly homogeneous wave conditions over the area scanned). Second, Jackson showed that the difficulties in the scattering microphysics problem encountered in the large angle Bragg-scatter regime could be avoided by operating the radar in the near-vertical, specular backscatter regime. Jackson pointed out that in the quasi-specular scatter regime near nadir, there is no dependence on the hydrodynamic modula-

[1] Now at Engineering Research Center, University of Maryland, College Park.

Paper number 4C1273.
0148-0227/85/004C-1273$05.00

TABLE 1. ROWS Instrument Characteristics

Parameter	Value
Frequency	13.9 GHz
Pulse type	linear FM, 100 MHz bandwidth, 1.2 μs chirp
Pulse length	12.5 ns compressed
Peak power	2 KW
PRF	100 Hz maximum
Dynamic range	70 dB
Detection	noncoherent, square law
Antenna	10° elevation by 4° azimuth beamwidth printed circuit array (vertically polarized), 16° boresight angle, 6 rpm rotation rate
Data	digital, maximum 1024 six bit word frame size, selectable sample gate widths, 2, 5, 10 ... *ns*, recording at full PRF

tion of a particular small Bragg-diffracting water wave: theoretically, he showed that hydrodynamic nonlinearity, to the extent that it affects the measurement, is a second-order effect, and that the scattering surface could be modeled adequately by Gaussian statistics. Further, under the appropriate (rather large) range of conditions, the specular scatter problem could be reduced to a simple, linear tilting model in which the reflectivity modulation is directly proportional to the large wave slopes.

Jackson's [1981] theory has been substantiated by *Jackson et al.* [this issue]—hereinafter referred to as *JWB*—with an extensive aircraft data set obtained with the NASA K_u-band radar ocean wave spectrometer (ROWS), an experimental prototype of a possible satellite instrument. In *JWB* it was shown on the basis of nondirectional buoy intercomparisons that the ROWS technique is capable of accurate measurements of absolute height spectra over a range of sea states from ~2 m to over 9 m significant wave height. In the present note, we offer a detailed analysis of the one directional intercomparison data set obtained during the fall 1978 aircraft mission (cf. *JWB*, Table 1). To date, this intercomparison, with a NOAA pitch-roll buoy, represents the only in situ directional intercomparison data we possess; the data are thus unique and deserving of a careful analysis. It will be shown that, despite certain discrepancies, the agreement between the ROWS and buoy spectra is remarkably good. Specifically, we find that there is excellent agreement overall in terms of the nondirectional height spectra, and mean wave directions and directional spreads as functions of frequency. This observation alone is noteworthy; however, we have also discovered, on paying these data closer attention, that the ROWS spectrum is remarkably similar to the clasical SWOP (stereo wave observation project) spectrum [*Coté et al.*, 1960]. The spectra, each representing ostensibly fully developed sea conditions, show a strong similarity in their directional characteristics, not only in terms of the gross spreading, but in terms of the detailed shape as well. In particular, both spectra are seen to exhibit what appear to be Phillips' resonance modes. The observation reported here thus represents both a unique verification (or replication) of the SWOP results and additional evidence pointing to the importance of the Phillips' resonance mechanism in maintaining the fully developed sea state.

The following description of the ROWS technique recapitulates that given in *JWB* with minor change. (Originally, this note was to appear in this journal without *JWB*, and so the discussion was designed to stand alone.) Those who have read *JWB* may therefore skim the following section.

NASA RADAR OCEAN WAVE SPECTROMETER (ROWS)

The GSFC K_u-band radar ocean wave spectrometer (ROWS) is a noncoherent, short pulse radar that uses a near-nadir directed conically scanning antenna to map wave directionality. Table 1 gives the pertinent instrument characteristics. Figure 1 depicts the aircraft measurement geometry. A small rotary antenna boresighted to 16° incidence produces a footprint at a nominal 10-km aircraft altitude measuring approximately 1500 m in the range (x) dimension and 700 m in the orthogonal azimuthal (y) dimension. The surface is probed in the range dimension using 12.5 ns compressed pulses. At the nominal incidence angle for peak power return, $\theta = 13°$, the surface range resolution is 8 m. The directional resolution of the ROWS is obtained by a simple phase front matching between electromagnetic wave and ocean Fourier contrast wave components across the relatively broad azimuth beamwidth. In a manner similar to a linear wave gauge array, the narrow illuminated strip on the surface (Figure 1) functions to isolate, or resolve, ocean Fourier components whose wave vectors $\mathbf{k} = (k, \phi)$ are prependicular to the strip and oriented in the radar's azimuth direction ϕ. In this respect, the ROWS technique is similar to the dual frequency technique investigated by *Plant* [1977], *Schuler* [1978], *Alpers and Hasselmann* [1978] and others. Let the fractional cross section variation for any pixel (x, y) be denoted $\delta\sigma/\sigma$. The fractional reflectivity modulation m seen by the radar is then given by $\delta\sigma/\sigma$ averaged laterally across the beam. If $G(y)$ denotes the lateral gain pattern, then

$$m(x, \phi) \equiv \delta W/W = \frac{\int G^2(y)(\delta\sigma/\sigma)\, dy}{\int G^2(y)\, dy} \qquad (1)$$

where $\delta W/W$ is the fractional variation in backscattered power versus range (averaged over the clutter fluctuations).

In the near-vertical specular backscatter regime in which the ROWS operates, the cross-section variation is due to the modulation of the specular point density and intercepted surface area by the slopes of the long underriding dominant waves. The modulation can be shown [*Jackson*, 1981] to be primarily a geometrical tilting effect, hydrodynamic modulation effects being of second order. Provided the large-wave steepness is small compared to the total surface roughness as measured by the total (diffraction-effective) mean square slope β^2, then the cross section variation will be proportional to the

RADAR OCEAN WAVE SPECTROMETER

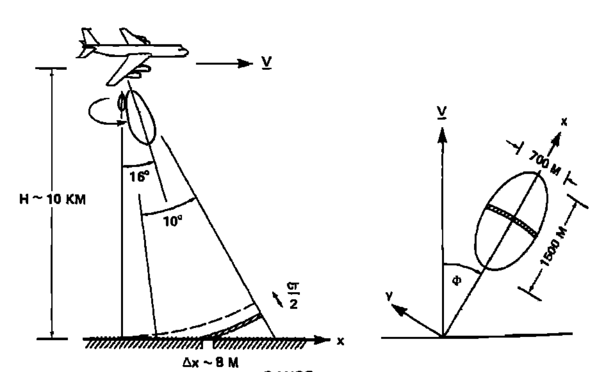

Fig. 1. Aircraft measurement geometry.

large-wave slope component in the plane of incidence $\partial\zeta/\partial x$ as

$$\frac{\delta\sigma}{\sigma} = \left(\cot\theta - \frac{1}{\sigma^0}\frac{\partial\sigma^0}{\partial\theta}\right)\frac{\partial\zeta}{\partial x} \tag{2}$$

where θ is the angle of incidence and $\sigma^0 = \sigma^0(\theta, \phi)$ is the average cross section of the surface. In (2) the first term represents a linearized area tilt term while the second term represents the rigid rotation of the small-scale scattered power pattern by the large wave slopes. The average cross section is proportional to the probability density function (pdf) of surface wave slopes evaluated at the specular condition for backscatter (namely, slope = tan θ). Assuming a Gaussian distribution of slopes symmetrical about the wind direction ϕ_w, the cross-section roll-off is given approximately by

$$\frac{1}{\sigma^0}\frac{\partial\sigma^0}{\partial\theta} = -\tan\theta\left[\frac{\cos^2(\phi-\phi_w)}{\beta_u^2} + \frac{\sin^2(\phi-\phi_w)}{\beta_c^2}\right] \tag{3}$$

where β_u^2 and β_c^2 are the upwind and crosswind mean square slope components. The total (diffraction-effective) mean square slope, $\beta^2 = \beta_u^2 + \beta_c^2$ is approximately a linear function of the surface wind speed U. In *JWB*, a wind speed dependence is inferred which is in good agreement with K_u-band scatterometer data analyzed by *Wentz* [1977]:

$$\beta^2 = 0.0028\ U[m/s] + 0.009 \tag{3'}$$

This relationship gives slope values which are about 60% of the optical values of *Cox and Munk* [1954], consistent with the fact that the capillary portion of spectrum lies under the diffraction limit for 2 cm radiation. At K_u-band, the slope pdf is nearly isotropic. *Wentz*'s [1977] data give an average ratio of crosswind to upwind mean square slope components equal to 0.88. Recently obtained ROWS data (unpublished) give about the same result (0.84).

Assuming that the water wavelength $2\pi/k$ is small compared to the azimuth beamwidth L_y, $kL_y \gg 1$, it follows from (1) and (2) that the spectrum of $m(x, \phi)$ is proportional to the directional wave slope spectrum. If the gain pattern is assumed to be Gaussian, $G(y) = \exp(-y^2/2L_y^2)$, one finds that, in the limit of large kL_y, the directional modulation spectrum is given by

$$P_m(k, \phi) = \alpha k^2 F(k, \phi) \tag{4}$$

where F is the directional height spectrum and α is the sensitivity coefficient given by

$$\alpha \equiv \alpha(\phi, \mathrm{U}) = \frac{\sqrt{2\pi}}{L_y}\left(\cot\theta - \frac{1}{\sigma^0}\frac{\partial\sigma^0}{\partial\theta}\right)^2 \tag{4'}$$

where U is the wind vector. In evaluating (4') for the aircraft data, we assume a nominal incidence angle of 13° corresponding to the nominal angle for peak power return over the 10° beamwidth (approximate center of range data window). The modulation spectrum is defined such that the modulation variance,

$$\langle m^2(x, \phi)\rangle = \int_0^\infty P_m(k, \phi)\, dk$$

and the height spectrum is defined such that the wave height variance

$$\langle\zeta^2\rangle = \int_0^\infty \int_0^\pi F(k, \phi)k\, dk\, d\phi$$

We note that in (1) the azimuth coordinate y was treated as rectilinear; this is permissible for directionally spread seas.

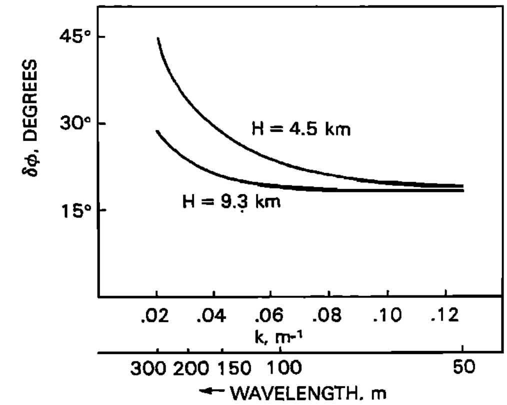

Fig. 2. Directional resolution (spectral half-power) versus wave number for two altitudes.

The wave front curvature enters, along with the finite footprint size and antenna rotation, in determining the directional resolution. The directional resolution for a stationary beam $\delta\phi_{stat}$ is given by equation (2) in *JWB*. In the case of a rotating beam in which an azimuth $\delta\phi_{rot}$ is swept out during the pulse integration time, one may approximate the resolution by

$$\delta\phi = [(\delta\phi_{stat})^2 + (\delta\phi_{rot})^2]^{1/2} \tag{5}$$

The directional resolution (spectral, half power) is graphed in Figure 2 as a function of wave number for two aircraft altitudes assuming $\delta\phi_{rot} = 15°$. At 9.3 km altitude, the resolution varies from 30° for a 300 m wavelength to 17° in the zero wavelength limit.

The ROWS data processing consists of first correcting for the wave front sphericity on a pulse by pulse basis on going from the signal delay time to the surface range coordinate x, and then integrating the pulse returns in surface-fixed range bins over a time corresponding to 15° of antenna rotation ($N = 42$ pulses). The surface tracking is accomplished using an input aircraft speed. The modulation $m(x, \phi)$ is then computed by normalizing by an estimate of the average power envelope $W_0(x, \phi) = \langle W(x, \phi)\rangle$. Unity is then subtracted and the data are rewindowed with a cosine-squared (Hanning) window and the spectrum $P_m(k, \phi)$ computed by a 256 point fast Fourier transform. The final estimates of P_m are obtained by averaging the spectra over several antenna rotations, subtracting a computed residual fading spectrum, and correcting for the finite pulse response. The result of this processing is to produce an estimate of the modulation spectrum given by

$$\hat{P}_m(k, \phi) = R^{-1}(k)[\hat{P}_N(k, \phi) - N^{-1}P_w(k)] \tag{6}$$

where $\hat{P}_N$ is the observed reflectivity spectrum for the N pulse ($N \equiv 42$) average, and $R(k)$ and $P_w(k)$ are respectively the pulse response function and computed background fading spectrum. For a Gaussian pulse shape,

$$\begin{aligned} R(k) &= \exp(-k^2/2k_p^2) \\ P_w(k) &= (2/\pi)^{1/2}k_p^{-1}R(k) \end{aligned} \tag{6'}$$

where in terms of the half-power range resolution Δx, $k_p = 2(\ln 2)^{1/2}/\Delta x$. At the nominal incidence angle $\theta = 13°$ for peak power return (approximate center of range data window), $\Delta x = 8.5$ m.

In the high altitude data (8–10 km), the geometrically corrected range data are arrayed in equally spaced 12 m range bins; in the low altitude range (4–6 km), the bin size is reduced to 6 m. In the process, the original 512 point data record is truncated to a 256 point record spanning $x = 800$–3872 m in the high altitude range and $x = 400$–1936 m in the low altitude range. In each case, the incidence angle varies from 5° to 21° approximately over the record. The record midpoint corresponds roughly to 13.5°, and the Hanning window half power points correspond to 9° and 17° approximately.

To increase the degrees of freedom (DOF) of the spectral estimates for each azimuth, the measured 360° directional modulation spectrum is symmetrized by averaging looks 180° apart; that is, the spectrum is symmetrized according to

$$\hat{P}_m(k, \phi) \leftarrow 0.5[\hat{P}_m(k, \phi) + \hat{P}_m(k, \phi + 180°)] \tag{7}$$

In addition to doubling the DOF of the estimates, this operation eliminates any real asymmetry that may exist in the modulation spectrum due to nonlinear effects (e.g., wave slope skewness) or possibly aircraft attitude errors. Finally, assuming the linear deep-water dispersion relationship, P_m is converted to a polar-symmetric directional height spectrum in the frequency domain according to the linear tilt model solution (4), namely,

$$S(f, \phi) = (2/\alpha f)P_m(k, \phi) \tag{8}$$

where S is defined such that the height variance $\langle \zeta^2 \rangle = \iint S(f, \phi)\, df\, d\phi$.

DATA PROCESSING CHANGES

The processing of the data reported here differs slightly from the data processing described in *JWB*.

1. In the windowing routine, the Hanning window endpoints are moved in from the ends of the 256 point range records by 40 six-meter bins on each end (near and far range) in order to avoid small data values and the effects of thresholding. The ends of the record are then blanked with zeros. The 3-dB resolution is then $1.44 \times (256/176) = 2.1$ transform bins and the wave number resolution is accordingly 1/1056 cpm (low altitude case) corresponding to which is a frequency resolution of

$$\delta f \sim 0.01 \text{ Hz, e.g., at } f = 0.12 \text{ Hz (peak frequency)}$$

2. The average power estimates $W_0(x, \phi)$ are here computed according to two algorithms. Algorithm I is identical to that in *JWB*. With the motion compensation disabled, the range data for each azimuth are averaged in 8 range bin intervals and then averaged over the successive rotations of the antenna. These data are then smoothed over adjacent azimuth bins with a (0.25, 0.50, 0.25) smoother and finally linearly interpolated over the 8 bin intervals. Concern over the effect of aircraft attitude variations on the average power estimate so computed has prompted us to try another average power routine, one that would be relatively immune to the gain pattern shifting caused by aircraft attitude changes. The shifting causes a misregistration and smearing of the average power envelope with respect to the individual turn power profile data; hence, the normalization will be incorrect. This problem is exacerbated by the presence of gain pattern anomalies associated with the antenna environment. The gain anomaly, of approximately 3° wavelength in the elevation plane, is variable with azimuth, and appears to be caused by the structural members of the instrument sled as well as the baffle around the antenna (cf. Figure 4 in *JWB*). Algorithm II estimates the average power envelope on an individual turn basis simply by smoothing in range and azimuth. The data are averaged in 16 or 32 bin (96 or 192 m) range intervals and smoothed in azimuth with the same weights as in algorithm I. These data are then cubic spline interpolated to yield a smooth average power profile estimate.

3. The data shown here have been corrected for the pulse response $R(k)$.

4. The sensitivity coefficient here is computed for two cases, (1) isotropic slope pdf and (2) anisotropic pdf, cross-wind/along-wind mean square slope axial ratio equal to 0.85.

PITCH-ROLL BUOY COMPARISON

A pitch-roll buoy of the *Cartwright* [1963] design was deployed at Ocean Weather Station PAPA in the N.E. Pacific (50° N, 145° W) during the time of overflight on November 17, 1978. Five buoy spectra of 0.008 Hz resolution and 28 degrees of freedom (DOF) obtained over the period 1811 UT to 2138 UT were kindly provided to us by W. McLeish and D. Ross of the NOAA Atlantic Oceanographic and Meteorological Laboratories. These spectra were in the form of nondirectional height spectra and first and second angular harmonic coefficients and associated spread parameters.

Two ROWS files (cf. Table 1 in *JWB*) were taken in the immediate vicinity of PAPA. File 89/2, of 1-min duration, was taken 6 km distant from PAPA at an altitude of 9.3 km; file 89/3, 1.5 min long, was taken at an altitude of 4.5 km at a distance of 42 km to the WNW of PAPA. We concentrate here on the longer 89/3 file and reserve the 89/2 file for an appendix, mainly on account of the greater statistical stability of the longer file, but also for reasons made evident in the appendix. The 89/3 file, consisting of nine antenna rotations, yields directional modulation spectrum estimates with 18 DOF, and polar symmetric height spectrum estimates of 36 DOF. Examination of the aircraft log verified constant head-

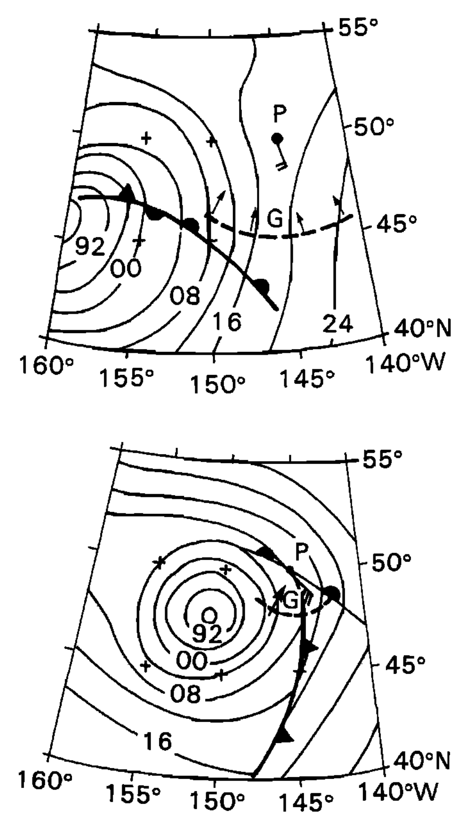

Fig. 3. Surface weather charts for (top) 0000 UT and (bottom) 1200 UT, Nov. 17, 1978. P is Weather Station Papa. The generating regions for 0.12 Hz wave packets arriving at Papa at the time of the measurements (ca. 2130 UT) are indicated by the dashed curves G.

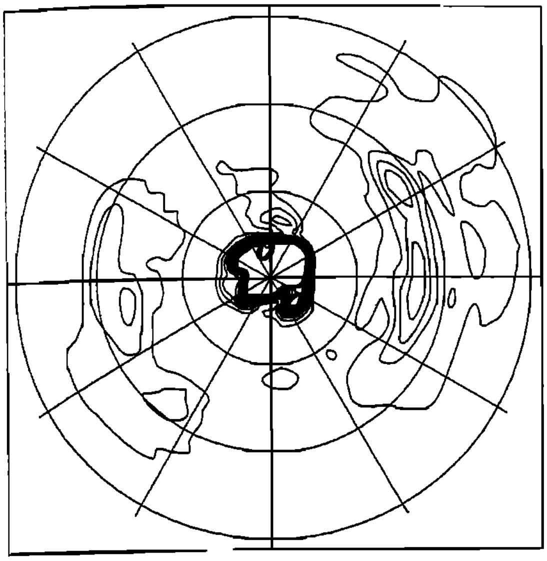

Fig. 4. Observed directional reflectivity modulation spectrum for file 89/3, algorithm I (but processed with old window end points). The wave number rings are 0.005, 0.01, and 0.015 cpm. The figure is oriented with the aircraft heading 96° T to the top of the page. The contour levels are equally space at intervals of 2.58 per meter.

ing for the duration of the file, but attitude changes in both pitch and roll of ca. $\pm 3°$ occurred during the data take.

The general meteorological situation and wave conditions at the time of the measurements have been described by *McLeish and Ross* [1983]. The synoptic charts in Figure 3 show a low pressure system approaching PAPA from the southwest, with the warm front reaching PAPA on the 1200 UT map. The winds at PAPA over the 24-hour period preceding the observations were southerly and fairly steady at 9–13 m/s. Initially southwesterly at 1800 UT on the 16th, the winds shifted gradually to southeasterly over the next 24 hours. Several hours before the data take, the winds dropped from 13 m/s to 9 m/s and assumed a direction from 130°. Despite the wind turning at PAPA, the basic picture from the weather charts is one of fairly constant southerly winds in the generating areas (labeled G on charts) to the south of PAPA. Thus, we might expect a fully developed spectrum similar to the SWOP spectrum. As reported by McLeish and Ross, the buoy-observed dominant wave frequency of $f = 0.12$ Hz and significant wave height of $H_s = 3.3$ m are consistent with fully developed conditions for the observed maximum winds of 13 m/s. The wind field variability appears to be qualitatively similar to that in SWOP; to the extent that wind field variability affects the form of the presently observed spectrum, it must also be considered to similarly affect the SWOP results. In fact, it is probable that the very close agreement we shall find with the SWOP results is due to the happenstance of very similar generating conditions (e.g., upfetch wind shear, falling winds).

Figure 4 is a polar contour plot of the observed directional modulation spectrum (computed according to the average power algorithm I). The figure indicates a fairly broadly spread (80°) sea of ~ 120 m wavelength with a mean direction toward the north (or south), and, in addition, an eastward (or westward) travelling ~ 300 m wavelength swell. The observed spread of the swell component in Figure 4 is about 45°. However, according to Figure 2, this is equal to the ROWS directional resolution for this wavelength and altitude, and so it can only be concluded that the swell angular spread is considerably less than 45°. In Figure 4 one can see some evidence of wind turning, or upfetch wind shear, with the spectrum slewing clockwise toward lower frequency. The spectrum also exhibits a weak bimodality. The asymmetry which is apparent in Figure 4, and also the large amount of low-frequency energy near the origin are noted. The excessive low-frequency energy is due primarily to the problems with the algorithm I average power normalization in dealing with the gain-pattern shifting caused by the aircraft attitude changes, which causes long wavelength antenna pattern energy to appear as modulation power. A typical example of the range signal is given in Figure 5. This example shows a slight misregistration of the average power with respect to the 42-pulse average signal; severe mismatching only occurred in the first and last few of the nine antenna rotations. Figure 6 shows the same range signal, and in addition, the signals from two adjacent azimuth bins, with the corresponding algorithm II average power envelopes (32 bins). The better fit of algorithm II is evident. In Figure 6, one sees only slight evidence of the gain pattern anomaly in the vicinity of the antenna boresight (ca. range bin 179). The anomaly is most severe near 0° and 180° (fore and aft directions); it is only accommodated well by algorithm II with 16 bin averages. An example of the modulation $m(x, \phi)$ (before windowing) corresponding to Figure 6 is given in Figure 7. Note that the signal appears to be stationary; this would indicate that the sensitivity is fairly uniform over the range.

An examination of the algorithm II spectra (for both 16 and 32 bin averages) shows them to be similar to the algorithm I spectrum of Figure 4. Thus, it does not appear that the spectrum is subject to any significant contamination by the gain anomaly and gain pattern shifting. The asymmetry then appears to be real and related to the asymmetry of (skewness of) the wave slope pdf. Since the sea is fully developed with a relatively mild 1/20 wave slope, the skewness must be due to the higher frequency waves which are subject to stronger wind forcing. However, we have not yet undertaken a systematic investigation of the modulation spectrum asymmetries (nonlinearities), and so our remarks here are somewhat speculative.

The symmetrized height spectrum (algorithm I, isotropic sensitivity) is shown in Figure 8. In this figure, the dc has been eliminated by the expedient of simply zeroing out (in the original modulation spectrum) all energy at wave numbers below the first encountered minimum in spectral density between the dc and the peak. In calculating the amplitude, a mean square slope $\beta^2 = 0.040$ is assumed based on the observed value of α,

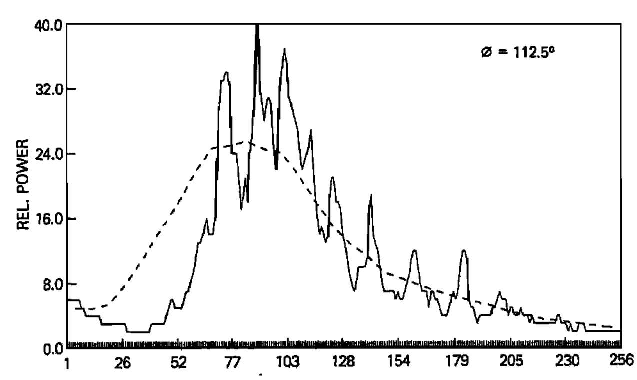

Fig. 5. Example of backscattered signal power versus surface range (15°, 42 pulse average power) for file 89/3, turn 5, azimuth bin 7, with algorithm I estimated average power envelope (dashed curve). The range bins are 6 m. Bin 1 is at a range $x = 400$ m from the nadir point.

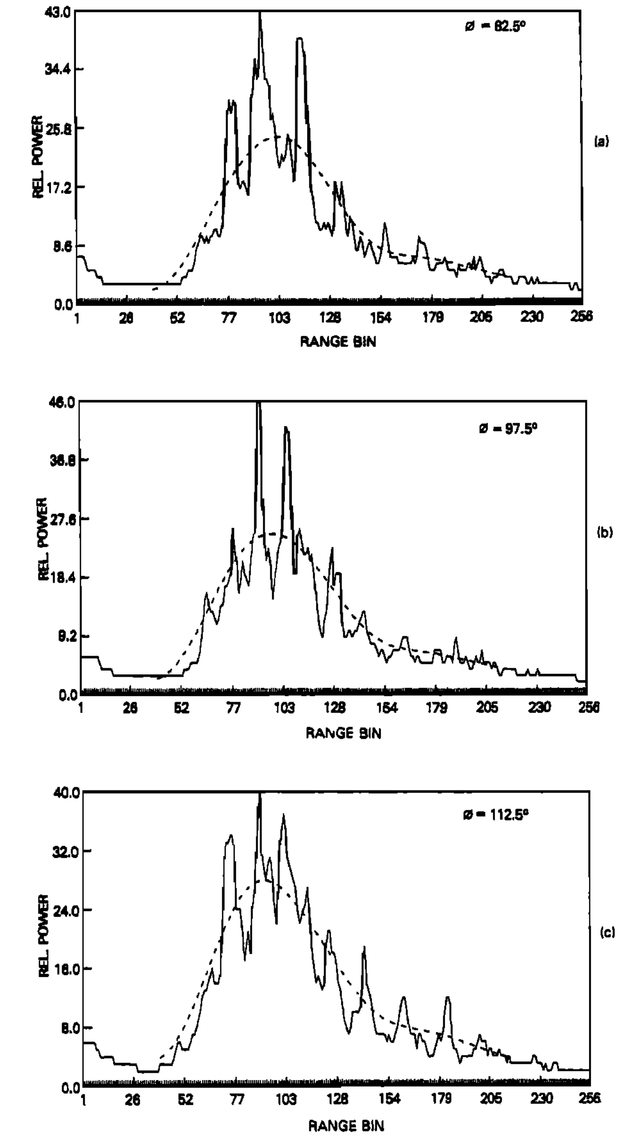

Fig. 6. Backscattered power profiles (15°, 42 pulse averages) for three adjacent azimuth bins near broadside look compared with the algorithm II average power estimates (dashed curves). The anomalous gain pattern can be seen in the tailed structure of the return and the slight bump near the boresight (ca. bin 179).

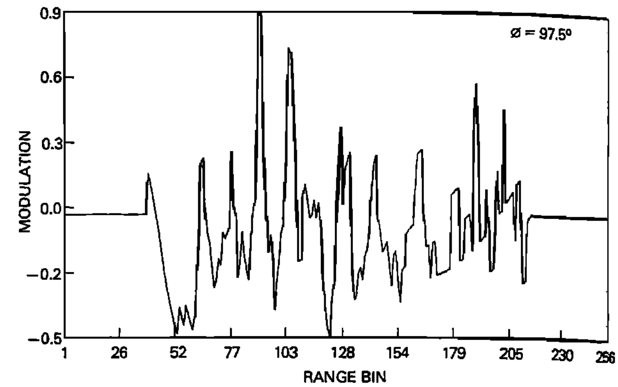

Fig. 7. Example of the normalized range reflectivity modulation signal computed from the data of Figure 6*b*. (Note: the numbers are not whole decimals—the second digit was lost in the figure. Zero level is given by level ends of the record.)

defined as the ratio of areas under the radar (unit α) and buoy spectra. From (3′), it is seen that this mean square slope value corresponds to a wind speed of 11.1 m/s, which is quite reasonable considering the observed wind speed ranged from 9–13 m/s prior to the observation. The height spectrum of Figure 8 shows bimodality at the peak. In earlier processed spectra, this bimodality was not evident; cf. Figure 11*d* in *JWB*.

Normalized directional distributions corresponding to the directional spectrum of Figure 8 are shown in Figure 9 (again, algorithm I data, isotropic α). The bimodality of the spectrum, the increasing separation of the modes with increasing frequency, and the general slewing of the spectrum into the local wind direction, to 310°, with increasing frequency are apparent from the distributions (the arrows give the locations of postulated Phillips' modes; see below). At frequencies below the peak frequency $f \sim 0.119$, bimodality also is evident. The right mode appears to be the rear face of the $\sim$0.075 Hz swell traveling toward 90° T. Note that in these distributions, adjacent frequencies are highly correlated.

The nondirectional height spectrum, $S(f) = \int S(f, \phi)\, d\phi$, (isotropic case) is shown in Figure 10 compared to the buoy spectra from the two closest records at 2104 UT and 2138 UT. In this comparison, we have averaged the two buoy spectra and, further, we have averaged the buoy spectra in frequency with a (0.25, 0.50, 0.25) running smoother. The 95% confidence intervals on the buoy have been computed assuming (incorrectly) a constant spectrum over the three point band. The buoy confidence limits in this presentation are comparable to the ROWS confidence limits, which have been computed according to the total degrees of freedom,

$$\mathrm{TDOF} = 36 \times \frac{[\sum_i S(f, \phi_i)]^2}{\sum_i S^2(f, \phi_i)} \qquad i = 1, 12$$

[*Coté et al.*, 1960]. It is seen that, apart from the low-amplitude swell component which has been eliminated from the ROWS spectrum, the agreement is excellent over the entire energy-containing band and out to twice the peak fre-

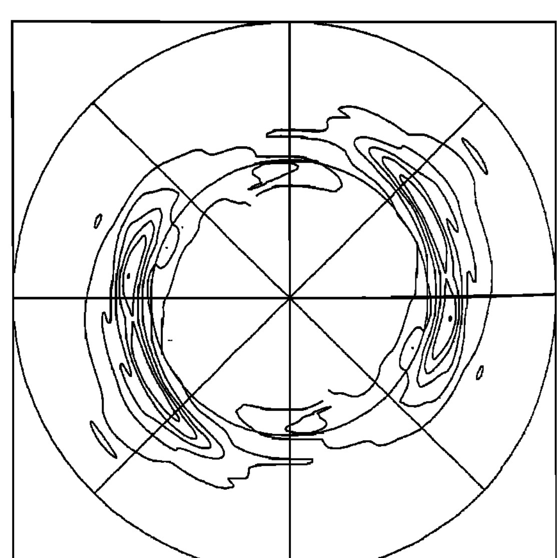

Fig. 8. ROWS inferred directional height spectrum. Frequency rings are 0.10 Hz and 0.20 Hz. Top of the figure is the aircraft heading, 96° true. The contour levels are equally spaced at intervals of 0.64 m^2/Hz/rad. The plot is for algorithm I data, isotropic sensitivity case.

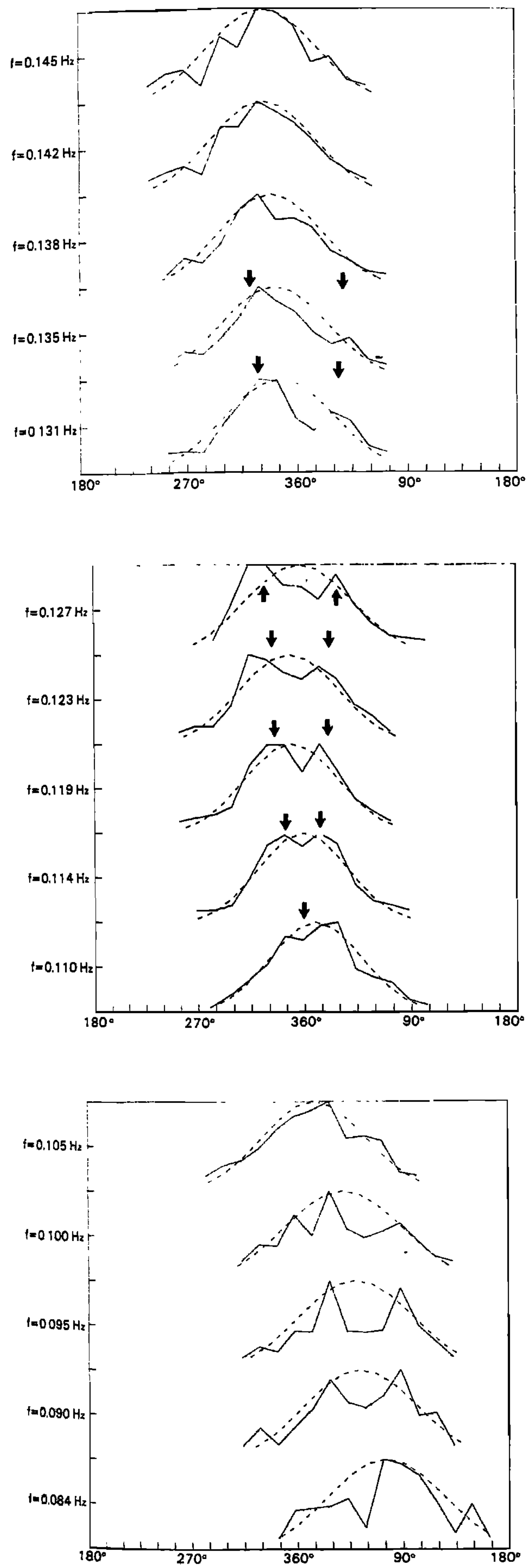

quency. (The swell component is resolved in the high-altitude data given in the appendix).

The observed spectrum is considerably sharper than the Pierson-Moskowitz (P-M) fully developed spectrum. It is in fact well-fitted by the JONSWAP spectrum [*Hasselmann et al.*, 1976] with the following parameter values: peak frequency $f_m = 0.12$ Hz, spread parameter $\sigma = \sigma_a = \sigma_b = 0.10$ Hz, peak enhancement factor $\gamma = 2.65$, and equilibrium constant $\alpha = \alpha_{PM}/2 = 0.00405$. The fitted spectrum is shown in Figure 10. The observed peakedness is not only large compared to the P-M spectrum (for which $\gamma = 1$), but is large as well compared to the average peakedness of the fully developed sea as determined by *Hasselmann et al.* [1976] based on their reanalysis of the P-M data ($\gamma = 1.4$). The sharpness of the peak in the present case may be due to the falling wind occasioning a transitioning of the sea to a more swell-like state. If the observation of the appendix (cf. Figure A2) is averaged with the present spectrum, then a (unimodal) spectrum results possessing a more rounded peak; the JONSWAP spectrum fit to this average spectrum gives $\gamma \sim 2$. (Most of the individual buoy spectra, it is noted, have extremely sharp peaks; see the example in *McLeish and Ross* [1983].)

The basic directional data provided by the buoy are the normalized first and second angular harmonic coefficients which are computed from the heave, pitch and roll sensor auto and cross spectra according to the method described by *Longuet-Higgins et al.* [1963] and *Cartwright* [1963]. A straightforward, objective comparison with the buoy data is possible in terms of the second harmonic values of the ROWS angular distributions. However, in the case of the first harmonics, the symmetrical radar distribution will only give zero unless an assumption about the true direction of wave travel is made. That is, one must assume that there are no reverse waves and that all wave propagation directions at any frequency are confined to 180°. Then the opposite half of the spectrum can be set to zero.

Let the spectrum be expressed as the product of the nondirectional spectrum $S(f)$ and a directional distribution $D(f, \phi)$,

$$S(f, \phi) = S(f)D(f, \phi)$$

where D is normalized so that $\int D \, d\phi = 1$. The harmonic expansion of D is expressed as

$$D = (1/2\pi) + (1/\pi) \sum_n [A_n \cos n\phi + B_n \sin n\phi] \qquad n = 1, 2, \cdots$$

Let ϕ_m be the angle of the minimum of the ROWS distribution for any frequency such that the true propagation directions are all supposed to lie in $(\phi_m, \phi_m + \pi)$. Then the signed distribution is given by

$$D_s = 2D \qquad \phi_m < \phi < \phi_m + \pi$$
$$D_s = 0 \qquad \text{otherwise}$$

The harmonics of the radar distribution are then computed

Fig. 9. Normalized directional distributions for the spectrum of Figure 8 for the frequencies indicated, azimuth of wave travel in degrees true. The confidence limits (90%) are given by 0.72 and 1.28 times the plotted values. The dashed curves are the cosine-power model fits based on the first harmonics of the distributions. The arrows indicate the Phillips' resonance angles. The wind direction is toward 310°.

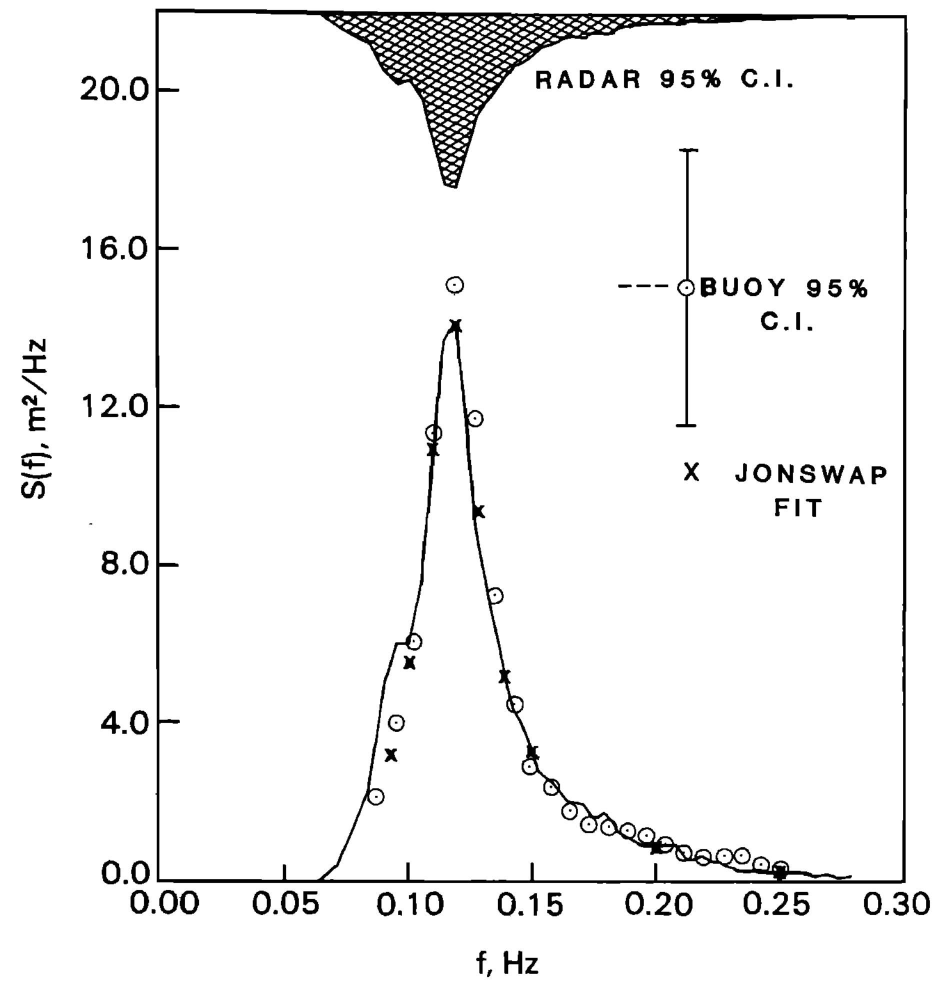

Fig. 10. Comparison of ROWS-inferred (solid curve) and buoy (circles) nondirectional height spectra (ROWS algorithm I isotropic data). The buoy spectrum is smoothed average of the two closest buoy records (2104 UT and 2138 UT). The hatched area at the top of the figure is the radar 95% confidence interval; the buoy confidence interval is indicated (for the peak only) by the vertical bar. The x are the values of the fitted JONSWAP spectrum.

according to

$$\begin{Bmatrix} A_n \\ B_n \end{Bmatrix} = \sum_{i=1}^{24} D_s(f, \phi_i) \begin{Bmatrix} \cos n\phi_i \\ \sin n\phi_i \end{Bmatrix} \times \frac{2\pi}{24}$$

The amplitudes and phases are given by $C_n^2 = A_n^2 + B_n^2$, $\phi_n = (1/n)$ atan (B_n/A_n), $n = 1, 2$. (Note that D need not be redefined for the even harmonics, and that properly it should not, as any noise in the location of the minimum may affect the result. However, we have carried out the computation also for the 360° symmetrial distribution and found no sensible effect on the resultant second harmonic amplitudes and phases).

Figure 11 compares the ROWS distribution first and second harmonic phases with the those of the closest buoy record at 2138 UT for both isotropic and anisotropic cases (algorithm I data). It is seen that there is basically excellent agreement, from the very forward face of the spectrum out to high frequency, although there appears to be a slight bias. According to *McLeish and Ross* [1983], the buoy compass card had slipped, and a correction had to be applied to the data based on a guess at the true mean direction; thus, one cannot attach any significance to any bias that may exist between the mean directions. We observe that the ROWS phase angles are nearly identical; the buoy mean directions are also close, but not quite so. In Figure 11*c*, it is seen that the overall agreement is improved somewhat if the average phase angles are compared.

Rather than directly compare the harmonic amplitudes, we will compare instead the associated spread parameters, as this proves to be a more informative comparison. A common practice in the analysis of pitch-roll buoy data is to assume a model function of the form,

$$D(f, \phi) = D_0 \cos^{2s} [(\phi - \phi_0)/2]$$

where D_0 is a normalization constant, and the spread parameter s and mean direction are functions of frequency. Two estimates of the spread parameter s_1 and s_2 are then obtained by equating the first two harmonic amplitudes of the model distribution $C_1(s)$ and $C_2(s)$ to the observed harmonics according to *Cartwright*'s [1963] formulae, namely,

$$C_1 = \frac{s}{1+s} \qquad C_2 = \left| \frac{s(s-1)}{(s+1)(s+2)} \right|$$

It follows that if the true distribution is perfectly modeled by the model function and the data are error free, then the two estimates of the spread parameter must be equal.

Figure 12 compares the ROWS and 2138 UT buoy record spread parameters (ROWS algorithm I isotropic case and algorithm II anisotropic case). It is seen that the ROWS s values are nearly equal and track each other closely over the entire

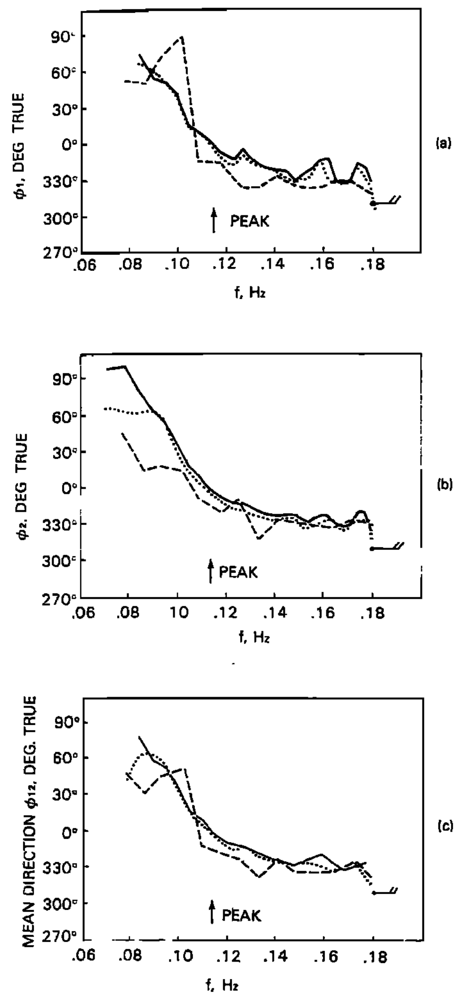

Fig. 11. Comparison of ROWS (algorithm I isotropic case, solid line; anisotropic case, dotted line) and buoy 2138 UT record (dashed line) first and second harmonic phase angles (Figures 11*a*, 11*b*) and average phase angles (Figure 11*c*).

range. At the peak, the ROWS $s_1 \sim s_2 = 4.5$; toward higher frequency the values decrease to about 2.5. The buoy s values on the other hand differ by a factor of 2–4 over most of the range and do not track each other well; obviously, the buoy s

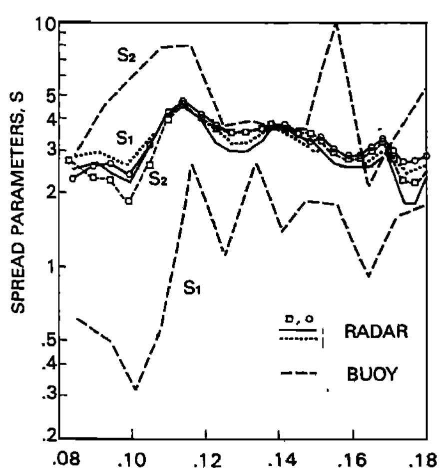

Fig. 12. Comparison of radar and buoy 2138 UT spread parameters. Solid and dotted curves are the ROWS algorithm I isotropic data: circles and squares are the algorithm II anisotropic data.

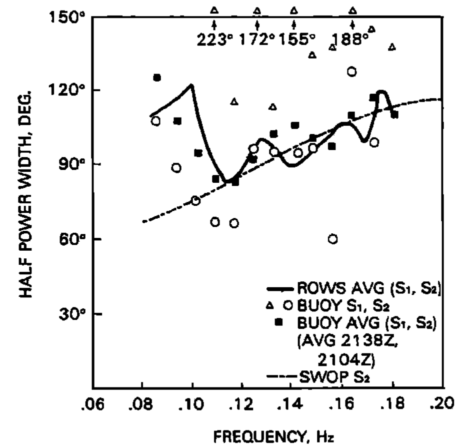

Fig. 13. Comparison of ROWS (algorithm I anisotropic data), buoy, and SWOP cosine-power model half-power spreads.

values are considerably noiser than the radar values. At the peak, the buoy $s_1 = 2.5$ and $s_2 = 8$. Relative to the ROWS values it appears that the buoy is overestimating s_2 and underestimating s_1. However, basically, over most of the range the agreement is better for s_2. This agreement is more apparent if we transform the spread parameters to half power widths (according to the cosine-power model). That is, let us compare the half power widths given by $\Delta\phi = 4\bar{a}$ cos $[(0.5)^{1/2s}]$. Figure 13 shows the comparison (algorithm I anisotropic results; the algorithm II results are nearly identical and are not plotted). Since the radar s-values are nearly equal, they have been averaged together before computing the half power spread. Also, in Figure 13, the ROWS data have been corrected for the finite resolution (cf. Figure 2) according to $\Delta\phi \leftarrow |\Delta\phi^2 - \delta\phi^2|^{1/2}$ (a minus 5° correction at the peak). It is seen that, overall, the s_2 agreement is good; on the high frequency side, except for the two wild buoy points the agreement is excellent; however, at the peak and on the forward face there appears to be significant disagreement on the order of 20–30%, the buoy spread being the narrower. The buoy s_1 spread on the other hand is quite large compared to the ROWS spread, with about half the buoy points exceeding 150°.

Ideally, the s_2 half power widths should agree, while the first harmonic widths need not necessarily agree. But, the question arises, why is the radar spectrum consistent with the cosine-power model while the buoy spectrum is not? It is seen in Figure 9 that the cosine-power model does indeed provide a good fit to the radar distributions, at least in the energy-containing part of the spectrum, despite the bimodality. Part of the reason the radar results agree so well with the cosine power model is that the radar spectrum (at any frequency) is constrained to lie within 180°, whereas the buoy spectrum is not. Thus, for example, reverse wave energy could substantially reduce the buoy first harmonic relative to the second [*McLeish and Ross*, 1983]. Another possible explanation is that the radar harmonics are derived from the same measured distribution (be it correct or no), whereas the buoy harmonics are derived from different sensor outputs. For example, relative phase lags between the acceleration and tilt sensors could reduce the first harmonic coefficients. The data of *Hasselmann et al.* [1980] support this hypothesis. Their Figure 10 comparing the harmonic coefficients computed from the vertical acceleration and inclination records to those computed from three-axis accelerometer records shows that the C_1 values from the sensor mix are significantly lower than the C_1 values

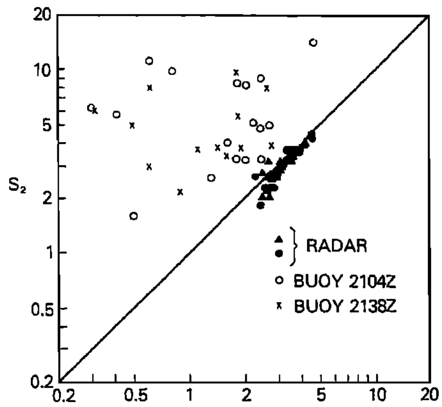

Fig. 14. Scatter plot of s_1 and s_2 spread parameters for radar and buoy.

from the three-axis accelerometer, especially on the forward face. Since the s_1 value is quite sensitive to small errors in the estimate of C_1, especially for the lower s values, a small reduction in C_1 will lead to a large reduction in s_1. The s_2 value is not as sensitive to errors in the C_2 estimates. However, according to *Hasselmann et al.* [1980], sampling variability will bias the estimate of C_2 high.

A scatter plot of s_1 versus s_2 for the ROWS and buoy data is given in Figure 14. The ROWS data are seen to cluster about the line of agreement, $s_1 = s_2$, while the buoy data are seen to exhibit a scatter pattern similar to that observed in *Cartwright*'s [1963] and *Hasselman et al.*'s [1980] data. E. J. Walsh (personal communication, 1984), in comparing surface contour radar (SCR) data [*Kenney et al.*, 1979; *Walsh et al.*, 1982] with data from two types of directional buoys, has found a similar pattern, with the SCR (symmetrical) spectra giving $s_1 \sim s_2$ while the buoy spread parameters scatter widely, in $s_1 < s_2$ in the case of one buoy and in $s_1 > s_2$ in the case of the other. In contrast to these buoy data sets, and in agreement with the SCR and ROWS observations, are the cloverleaf buoy observations of *Mitsuyasu et al.* [1976], which give $s_1 \sim s_2$ with little scatter. Thus, while it is possible for there to be a tendency for s_2 to scatter high relative to s_1 in the buoy observations due to reverse waves as suggested by *McLeish and Ross* [1983], there is good reason to suppose that this behavior is due to buoy instrumental effects.

Cartwright [1963], noting the tendency of s_2 to scatter high relative to s_1, suggested that, in the absence of any reason to prefer one harmonic to the other, the two s values might simply be averaged. From Figure 12, it might be expected that this procedure will lead to a better overall agreement. The comparison given in Figure 13, in terms of the half power spreads, shows this to be the case. For this comparison, we have, in addition to averaging the buoy s values, averaged the resultant half power spreads from the 2104 UT and 2138 UT buoy records, and further applied a three point smoother. Thus, this comparison is consistent with the nondirectional spectrum comparison of Figure 10.

SON OF SWOP

A comparison of the present ROWS spectrum with the SWOP spectrum (cf. Figure 11.16 in *Coté et al.* [1960] and Figure 1 in *Phillips* [1958]) shows such a close family resemblance that it is tempting to call our spectrum "The Son of SWOP". Both spectra exhibit a similar bimodality and as a consequence have a square shouldered appearance. The actual measured half-power widths agree within 5° at the peak (80° for the (resolution-corrected) ROWS and 75° for the SWOP; 70° for the ROWS just below the peak at 0.11 Hz). Also, both spectra exhibit to a similar degree the effects variability in the generating wind fields. These effects are perhaps most clearly seen in the slewing of mean direction with frequency: Compare Figure 11 with Figure 11.20 in the SWOP report.

The SWOP model function for the angular spread about the mean wind direction ($\phi = 0$) is

$$D_s(f, \phi) = (1/\pi) \times \{1 + [0.5 + 0.82\ Q(f)] \cos 2\phi + 0.32\ Q(f) \cos 4\phi\} \qquad |\phi| < \pi/2$$

$$D_s(f, \phi) = (1/\pi) \times 0 \qquad \text{otherwise}$$

where $Q(f) = \exp[-(2\pi f U/g)^4/2]$ (g being the acceleration of gravity and U the wind speed). The second harmonic of this distribution is

$$C_2 = 0.25 + 0.41\ Q(f)$$

Computing the associated s_2 parameter and the corresponding half power spread we arrive at the result given in Figure 13. It is seen that the SWOP result agrees very well with the ROWS and buoy spreads from the peak outward; however, on the forward face, the SWOP model function appears to underestimate the spread. Since an increasing spread on the forward face is a commonly observed property of wind-sea spectra [*Hasselmann et al.*, 1980], it is not peculiar to the present observation; hence, it appears to be the SWOP model function that is misrepresenting the spread on the forward face. (However, contamination by the swell may be broadening the forward face region of the present spectrum).

Phillips [1958] saw the bimodality of the SWOP spectrum as evidence of his resonance mechanism of wave generation. He noted the consistent trend of the modal angular separation with frequency in accordance with the resonance condition, and further noted that no other known mechanism of wave generation could explain this behavior. Subsequently, Phillips was criticized (comment by Cox following his paper; the SWOP report) for putting too much stock in a single observation: Conceivably, the modes could be a statistical artifact or a peculiarity of the generating wind field. Our observation will show that Phillips' original observation was correct, as it is highly unlikely that the same statistical fluke should occur twice under entirely independent conditions.

The Phillips' resonance mechanism is the resonant forcing of a wave component by convected turbulent pressure fluctuations. Resonance occurs when the wavelengths and frequencies are matched; or, when the component of the wind vector at some level $z \sim \pi/k$ in the direction of the water wave propagation equals the phase speed of the wave; that is, when

$$U_c \cos \gamma = c(f) = g/2\pi f$$

where U_c is the convection velocity, γ is the "resonance" angle, and c is the water wave phase speed. In Figure 9, the modes as given by the resonance angles, assuming a $U_c = 14.19$ m/s to give $\gamma = 0$ at $f = 0.11$ Hz, are indicated by arrows. These are placed symmetrically about an assumed mean wind direction of 352.5°. The resonance angles are seen to be quite close to the observed distribution modes, at least over the range from the peak to 0.135 Hz where the modes are distinct. Beyond this range, the right mode disappears while the left mode becomes the single dominant mode. This behavior is evidently due to the wind turning (the stronger, left mode lies closest to the local wind direction, to 310°). An asymmetry in modal

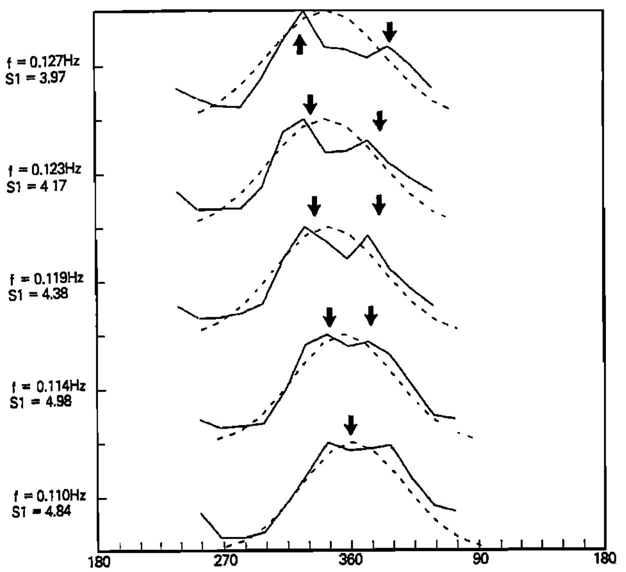

Fig. 15. Directional distributions, algorithm II data, for comparison with Figure 9.

amplitudes is also seen in the SWOP spectrum which also appears to be related to upfetch wind shear. Figure 15 shows the comparable results for the algorithm II data.

Usually, the Phillips' resonance mechanism is thought to be relevant to wave generation only in the initial stages of growth. However, it may be just as or more important in the final stages of growth, where the phase speed approaches the wind speed. In the initial growth stage ($c \ll U$), the forcing by the uncoupled atmospheric turbulent pressure fluctuations is actually nonresonant, except for wave components at very large angles to the wind; the growth is weak, and only serves to trigger the main stage of growth by the Miles' coupled shear flow mechanism. *Hasselmann* [1963] pointed to the likely importance of the Phillips' mechanism in the fully, or near fully developed sea state, noting that only in this case could one have truly resonant forcing of the energetic components travelling within moderate angles to the wind. He noted also that since the turbulent excitation is relatively stronger for the lower wave numbers for which $c \sim U$, the Phillips' mechanism may be particularly effective in the fully developed state. Further, since dissipation decreases as the significant wave slope relaxes toward full development [cf., *Huang*, 1984], the energy flux required to maintain the sea state may not be that great. Lastly, if (if underscored) the Miles' mechanism ceases to be effective when $c = U$, then the Phillips' mechanism must perforce be the responsible mechanism for maintaining the fully developed sea state.

Apart from the SWOP observation and the present observation, the only other observations of Phillips' resonance modes appear to be those of *Gilchrist* [1966] and of *Trizna et al.* [1980]. Gilchrist, using a gauge array in shallow water at small fetches, found only one mode, apparently because of the asymmetry in the fetch conditions. Trizna et al., using a coastal HF radar, found pronounced resonance modes only for short wind durations, attributing the lack of observable modes for the longer wind durations to the transition to Miles' growth. As the available observational evidence for the resonance modes is so scanty, we shall, in the future, examine all ROWS data for further evidence of the resonance mechanism, especially in observations of both early and late wave growth stages.

CONCLUSION

The directional spectrum of an essentially fully developed ~3 m sea as measured by an experimental airborne radar system, the NASA radar ocean wave spectrometer (ROWS) has been compared to reference pitch-roll buoy data and to the classical SWOP spectrum. We have found excellent agreement between the radar-inferred and buoy spectra; specifically, we have shown excellent agreement between the absolute nondirectional height spectra, and mean wave directions and directional spreading as functions of frequency. The most objective comparison of directional spread, that based on the second angular harmonic coefficients, gave excellent agreement above the peak, but at the peak a discrepancy in half power widths of about 20% was found, with the buoy the narrower. The buoy first harmonic spreads, on the other hand, were found to be very broad compared to the radar spreads; this discrepancy is attributed primarily to buoy instrumental effects. It was found that the best overall agreement was obtained by averaging the two buoy cosine-power spread parameters, although we could offer no reason why this should be the case.

This comparison is the first such to demonstrate the ability of a truly remote microwave radar technique to measure accurately the two dimensional wave energy spectrum. Most importantly, the technique is suitable for satellite application [*Jackson*, 1981; *JWB*]. Thus, measurements of the sort and of the quality of that reported here are potentially available on a global basis.

The present observation was seen to be very similar to the SWOP spectrum in detailed shape as well as in the gross spreading characteristics. The bimodality of the observed ROWS spectrum indicates that the SWOP spectrum bimodality was not a statistical fluke and that *Phillips* [1958] was correct in attributing the bimodality to the resonance mechanism. However, some caution should be exercised in interpreting these results. The broadly spread SWOP form may only be valid for very large fetch and duration; the behavior of the spectrum in the final stages of growth is unknown [*Hasselmann et al.*, 1976], and it should not be supposed that the SWOP form will hold simply because the phase speed and wave height have reached approximately fully developed values. A longer time may be required for the directional adjustment. Recently obtained ROWS data for large fetches [*Jackson*, 1984] indicate that this is the case. These data show wave heights and phase speeds close to the fully developed values, but the directional spreading is considerably narrower than the SWOP spread. Likewise, we do not know how often we may expect to find distinct resonance modes in the variety of seaways that may be characterized as "essentially" fully developed: Clearly, more observations are needed. The observation of Appendix underscores this point, as in that observation the modes are not at all apparent. A final caveat: the observed modes may not be produced by the Phillips resonance mechanism alone: The nonlinear spectral transfer function [e.g., *Fox*, 1978] shows a lobed structure that looks rather much like it could produce the kind of directionality observed here.

While we are continuing to validate the ROWS technique—principally with high-resolution directional spectrum data from the NASA Surface Contour Radar [*Kenney et al.*, 1979; *Walsh et al.*, 1982]—it is clear that we are at the point where we can apply the highly mobile aircraft system to basic waves physics investigations; for instance, the ROWS can be applied to solving the fundamental problems referred to in the introduction.

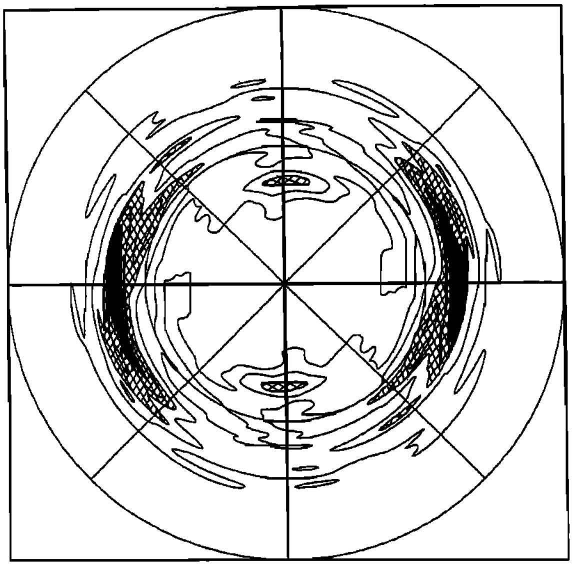

Fig. A1. ROWS file 89/2 directional height spectrum (isotropic case). The top of the page is the aircraft heading, 267° true. The contour levels are equally space at intervals of 0.52 $m^2/Hz/rad$; hatched area is 50% or more of the peak value, solid area is 83% or more of the peak.

APPENDIX

An additional ROWS file (89/2) is available for comparison. It was not included in the main report because first, being shorter than the file (89/3) chosen for the main report (1.0 vs. 1.5 min) it is noiser (DOF = 12 vs. 18); second, this file has some peculiar characteristics which, while not so peculiar as to contradict the 89/3 analysis results, are nevertheless peculiar enough that it was felt best, for the sake of clarity, to reserve this observation for an appendix. The 89/2 file was obtained at 2136 UT, 6 km distant from PAPA at an altitude of 9.3 km. Thus it is actually closer to the buoy than the 2143 UT 89/3 file, and at a more ideal altitude from a resolution point of view.

The unsmoothed directional spectrum from 89/2 is too noisy to make a presentable contour plot; hence, a smoothed version of the spectrum is given in Figure A1 (isotropic alpha case; 9 point symmetrical smoother in f-ϕ space, center weight = 1/2). It is seen that, basically, this spectrum is quite similar to that of Figure 8, having a nearly identical half power contour. It differs from the 89/3 observation in the detailed structure of the peak region, and in the swell region, where on account of the higher altitude of the 89/2 file, the definition is better (recall that in the 89/3 height spectrum the swell signature was eliminated because of its proximity to the dc pedestal). Curiously, however, the half power width of the

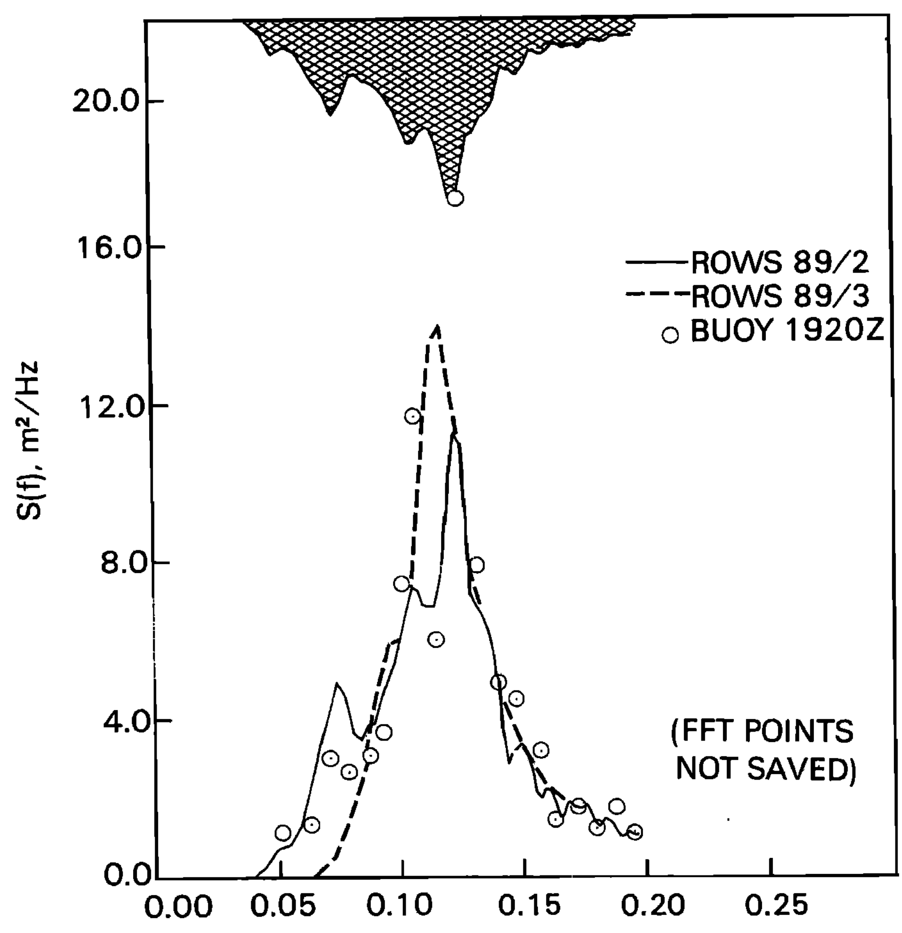

Fig. A2. ROWS file 89/2 "anomalous" nondirectional height spectrum compared to the "canonical" 89/3 spectrum and an "anomalous" buoy record at 1920 UT. The hatched area gives the 95% confidence interval for the radar data.

peak (at 0.075 Hz) is no narrower than the low altitude 89/3 observation, both observed widths being 45°. Since, according to *McLeish and Ross* [1983], the swell is from a distant storm, the angular width should be quite narrow, and so the observed spread should be close to the 30° resolution of the 89/2 observation (Figure 2, 300 m wavelength). Since the ROWS resolution has been verified for unidirectional swell (*JWB*) we do not believe there is a basic problem with the resolution prediction; conceivably, the apparent broadening is due to residual antenna pattern anomaly energy, which at this altitude has a wavelength comparable to that of the swell (300 m). In the wind-sea spectrum peak region, it is seen that relative to Figure 8 the spectrum of Figure A1 shows a slight shift of the left mode (viewed following the direction of propagation) to higher frequency from 0.118 Hz to 0.125 Hz, and the right mode appears to split into two components with frequencies of 0.108 Hz and 0.123 Hz. This behavior does not appear to be explained by resolution differences or by sampling variability.

Figure A2 shows the 89/2 nondirectional spectrum compared to the 89/3 observation (which, from Figure 10, is essentially the same as the combined 2104 UT and 2138 UT reference buoy observations) and to a buoy record taken at 1920 UT. The swell portion of the 89/2 spectrum is seen to compare fairly well with the buoy in absolute energy. The wind-sea peak is seen to be bimodal, with separate peaks at 0.105 Hz and 0.125 Hz. This bimodal structure appears to be truly anomalous, as four out of five buoy records and the 89/3 radar observation (the canonical observation) show only a single, well-defined peak. On account of the data window taper, the frequency resolution is about two transform bins, and so a doublet structure such as seen in 89/2 will tend to be smeared in the lower-altitude 89/3 file with only half the resolution. However, the buoy spectra all except for the plotted 1920 UT observation, show also only a single peak, and so the difference between the anomalous 89/2 radar and 1920 UT buoy spectra and the canonical observations does not seem to be due to resolution differences. An application of the F test at 99% significance to the ratio of anomalous and canonical samples at the frequency $f = 0.12$ Hz shows that it is unlikely for the anomalous and canonical observations to come from the same population. That the 89/2 observation is actually closer to the buoy than the canonical observation argues against large-scale geophysical variability as an explanation for the difference in peak structures; rather, it suggests that the difference may be due to nonlinear modulations acting on shorter scales.

Acknowledgments. We thank Duncan Ross and Bill McLeish of the NOAA Atlantic Oceanographic and Meteorlogical Laboratories for providing the buoy data. Paul Baker was responsible for the original ROWS software development. This work has been supported by funding from the Oceanic Processes Branch of NASA Headquarters.

REFERENCES

Alpers, W., and K. Hasselmann, The two-frequency microwave technique for measuring ocean wave spectra from an airplane or satellite, *Boundary Layer Meteorol.*, *13*, 215–230, 1978.

Alpers, W., D. B. Ross, and C. L. Rufenach, On the detectability of ocean waves by real and synthetic aperture radars, *J. Geophys. Res.*, *86*, 6481–6498, 1981.

Cartwright, D. E., The use of directional buoys in studying the output of a wave recorder on a moving ship, in *Ocean Wave Spectra*, pp. 203–218, Prentice-Hall, Englewood Cliffs, N.J., 1963.

Coté, L. J., J. O. Davis, W. Marks, R. J. McGough, E. Mehr, W. J. Pierson, Jr., J. F. Ropeck, G. Stephenson, and R. C. Vetter, The directional spectrum of a wind generated sea as determined from data obtained by the Stereo Wave Observation Project, New York University College of Engineering, *Meteorol. Pap.*, *2*(6), 88 pp., 1960.

Cox, C., and W. Munk, Measurement of the roughness of the sea surface from photographs of the sun's glitter, *J. Opt. Soc. Am.*, *44*, 838–850, 1954.

Dean, R. G., (Ed.), *Measuring Ocean Waves*, Marine Board, National Academy of Sciences, National Academy Press, Washington, D. C., 1982.

Fox, M. J. H., On the nonlinear transfer of energy in the peak of a gravity wave spectrum, in *Turbulent Fluxes through the Sea Surface, Wave Dynamics, and Prediction*, edited by A. Favre and K. Hasselmann, pp. 219–234, Plenum, New York, 1978.

Gilchrist, W. R., The directional spectrum of ocean waves: An experimental investigation of certain predictions of the Miles-Phillips theory of wave generation, *J. Fluid Mech.*, *29*(4), 795–816, 1966.

Hasselmann, D. E., M. Dunkel, and J. A. Ewing, Directional wave spectra observed during JONSWAP 1973, *J. Phys. Oceanogr.*, *10*(8), 1264–1280, 1980.

Hasselmann, K., Discussion, in *Ocean Wave Spectra*, pp. 132–134, Prentice-Hall, Englewood Cliffs, N. J., 1963.

Hasselmann, K., D. B. Ross, P. Muller, and W. Sell, A parametric wave prediction model, *J. Phys. Oceanogr.*, *6*(2), 200–228, 1976.

Hasselmann, K., (Ed.), Sea wave modelling report, in *Proceedings of Symposium on Wave Dynamics and Radio Probing of the Ocean Surface*, Plenum, New York, in press, 1984.

Holthuijsen, L. H., Observations of the directional distribution of ocean wave energy in fetch-limited conditions, *J. Phys. Oceanogr.*, *13*(2), 191–207, 1983.

Huang, N. E., An estimate of the influence of breaking waves on the dynamics of the upper ocean, in *Proceedings of Symposium on Wave Dynamics and Radio Probing of the Ocean Surface*, Plenum, New York, in press, 1984.

Jackson, F. C., An analysis of short pulse and dual frequency radar techniques for measuring ocean wave spectra from satellites, *Radio Sci.*, *16*, 1385–1400, 1981.

Jackson, F. C., Some case studies of ocean wave physical processes utilizing the GSFC Radar Ocean Wave Spectrometer, Proceedings of URSI Commission F Symposium and Workshop on Frontiers of Remote Sensing of the Oceans and Troposphere, Shoresh, Israel, May 14–23, 1984, *NASA Conf. Publ.*, *2303*, 233–246, 1984.

Jackson, F. C., W. T. Walton, and P. L. Baker, Aircraft and satellite measurement of ocean wave directional spectra using scanning-beam microwave radars, *J. Geophys. Res.*, this issue.

Kenney, J. E., E. Uliana, and E. J. Walsh, The surface contour radar, a unique remote sensing instrument, *IEEE Trans. Microwave Theory Tech.*, *MTT-27*(12), 1080–1092, 1979.

Kuik, A. J., and L. H. Holthuijsen, Buoy observations of directional wave parameters, in *Directional Wave Spectra Applications*, edited by R. L. Wiegel, pp. 61–70, American Society of Civil Engineers, New York, 1982.

Longuet-Higgins, M. S., D. E. Cartwright, and N. D. Smith, Observations of the directional spectrum of sea waves using the motions of a floating buoy, in *Ocean Wave Spectra*, pp. 111–132, Prentice-Hall, Englewood Cliffs, N. J., 1963.

McLeish, W., and D. B. Ross, Imaging radar observations of the directional properties of ocean waves, *J. Geophys. Res.*, *88*(C7), 4407–4420, 1983.

Mitsuyasu, H., F. Tasai, T. Suhara, S. Misuno, M. Ohkusu, T. Honda, and K. Rikiishi, Observations of the directional spectrum of ocean waves using a cloverleaf buoy, *J. Phys. Oceanogr.*, *5*(4), 750–760, 1976.

Pawka, S. S., S. V. Hsiao, O. H. Shemdin, and D. L. Inman, Comparisons between wave directional spectra from SAR and pressure arrays, *J. Geophys. Res.*, *85*(C9), 4987–4995, 1980.

Phillips, O. M., On some properties of the spectrum of wind-generated ocean waves, *J. Mar. Res.*, *18*, 231–245, 1958.

Plant, W. J., Studies of backscattered sea return with a CW, dual-frequency X-band radar, *IEEE Trans. Antennas Propag.*, *AP-25*, 28–36, 1977.

Schuler, D. L., Remote sensing of directional gravity wave spectra and surface currents using a microwave dual-frequency radar, *Radio Sci.*, *13*, 321–331, 1978.

Trizna, D. B., R. W. Bogle, J. C. Moore, and C. M. Howe, Observation by HF radar of the Phillips resonance mechanism for generation of wind waves, *J. Geophys. Res.*, *85*(C9), 4946–4956, 1980.

Walsh, E. J., D. W. Hancock III, D. E. Hines, and J. E. Kenney, Surface contour radar remote sensing of waves, in *Directional Wave*

Spectra Applications, edited by R. L. Wiegel, pp. 281–298, American Society of Civil Engineers, New York, 1982.

Wentz, F. J., A two-scale scattering model with application to the JONSWAP '75 aircraft microwave scatterometer experiment, *Contract. Rep. CR-2919*, NASA, 1977.

F. C. Jackson, Laboratory for Oceans, NASA Goddard Space Flight Center, Code 671, Greenbelt, MD 20771.

C. Y. Peng, Science Systems and Applications, Inc., Aerospace Building, 10210 Greenbelt Road, Seabrook, MD 20706.

W. T. Walton, Engineering Research Center, University of Maryland, College Park, MD 20742.

(Received April 23, 1984;
accepted July 17, 1984.)